Cellular and Molecular Bioengineering, Vol. 10, No. 4, August 2017 *(© 2017)* pp. 313–325
DOI: 10.1007/s12195-017-0488-5

Oxidative Stress Alters the Morphological Responses of Myoblasts to Single-Site Membrane Photoporation

XINXING DUAN,[1,3,4] JENNIFER M. F. WAN,[4] and ARTHUR F. T. MAK[1,2,3]

[1]Division of Biomedical Engineering, The Chinese University of Hong Kong, Shatin, Hong Kong; [2]Department of Electronic Engineering, The Chinese University of Hong Kong, Shatin, Hong Kong; [3]Department of Mechanical & Automation Engineering, The Chinese University of Hong Kong, Shatin, Hong Kong; and [4]School of Biological Sciences, The University of Hong Kong, Pokfulam Road, Hong Kong

(Received 7 October 2016; accepted 26 April 2017; published online 3 May 2017)

Associate Editor Richard Dickinson oversaw the review of this article.

Abstract— The responses of single cells to plasma membrane damage is critical to cell survival under adverse conditions and to many transfection protocols in genetic engineering. While the post-damage molecular responses have been much studied, the holistic morphological changes of damaged cells have received less attention. Here we document the post-damage morphological changes of the C2C12 myoblast cell bodies and nuclei after femtosecond laser photoporation targeted at the plasma membrane. One adverse environmental condition, namely oxidative stress, was also studied to investigate whether external environmental threats could affect the cellular responses to plasma membrane damage. The 3D characteristics data showed that in normal conditions, the cell bodies underwent significant shrinkage after single-site laser photoporation on the plasma membrane. However for the cells bearing hydrogen peroxide oxidative stress beforehand, the cell bodies showed significant swelling after laser photoporation. The post-damage morphological changes of single cells were more obvious after chronic oxidative exposure than that after acute ones. Interestingly, in both conditions, the 2D projection of nucleus apparently shrank after laser photoporation and distanced itself from the damage site. Our results suggest that the cells may experience significant multi-dimensional biophysical changes after single-site plasma membrane damage. These post-damage responses could be dramatically affected by oxidative stress.

Keywords—Cell morphology, Oxidative stress, Plasma membrane damage, Femtosecond laser photoporation, Single cell wound response.

ABBREVIATIONS

DM	Dichroic mirror
EOM	Electro-optic modulator
Fs	Femtosecond
NA	Numerical aperture
NCD	The distance between the nucleus center and the membrane damage site
PP	Photoporation

INTRODUCTION

Cells, such as muscle cells, are frequently subjected to physical and chemical stresses, which may lead to damages of the plasma membrane.[1,2] To survive the plasma membrane damage, cells have evolved a cascade of cellular responses to repair the disrupted membrane and to adapt to the environment, such as membrane patching and cytoskeleton reorganization around the wound site.[3–5] Such wound responses were usually considered as relatively localized processes. Recent studies showed that the disruption of plasma membrane could stimulate cytoskeletal reorganization quite distant from the wound site.[6] These results indicated that the process of plasma membrane disruption and repair might involve distant cellular responses apart from those in the immediate neighborhood around the wound site. Besides the involvement of massive intracellular molecules in the cellular wound responses,[7–9] more downstream insights in a biophysical context are necessary to bridge the gap between the molecular mechanisms and the overall cellular response patterns. Such information may provide an integrative perspective for a holistic understanding of cellular wound responses, and may potentially enhance the related therapeutic practice in drug delivery and gene transfection.

Address correspondence to Arthur F. T. Mak, Department of Electronic Engineering, The Chinese University of Hong Kong, Shatin, Hong Kong. Electronic mail: arthurmak@cuhk.edu.hk

An equally important aspect of understanding cellular wound responses is the micro-environmental conditions that the cells are frequently exposed to in their wounded situations. Oxidative stress is one of them.[10] Oxidative stress can alter many cellular functions and if excessive may lead to cell death.[11–13] In muscles, oxidative stress is associated with chronic pathology such as inflammations, degeneration and so on.[14,15] Little information is available on how oxidative stress may influence the responses of a cell to the physical damage on its plasma membrane.

In this study, we quantitatively investigated the morphological responses of single cells to plasma membrane perforation under normal and oxidative conditions. Various approaches have been developed to temporarily disrupt the plasma membrane for drug delivery and other biomedical applications, such as electroporation,[16] sonoporation,[17] and micropipette injection.[18] We chose femtosecond (fs) laser photoporation as the method for membrane disruption, for its being site-specific, highly focal (on the order of femtolitres), and dose-controllable. This allows membrane damage with high temporal and spatial specificity as well as with minimal collateral damage.[19,20] We established a biophysical model by reconstructing 3D plasma membrane topology and analyzed the wound responses of single myoblasts accordingly. We then compared the morphological responses of single myoblasts to fs-laser induced micro-damage on the plasma membrane under different oxidative conditions. To the best of our knowledge, this is the first integrative attempt to quantitatively investigate the 3D physical responses of single cells to a single-site plasma membrane wound on account of extracellular oxidative conditions.

MATERIALS AND METHODS

Laser Photoporation Platform and Protocol

The experimental setup is shown in Fig. 1. A Ti: Sapphire mode-locked fs laser (MaiTai HP, Spectrum Physics Inc.) was coupled with a fluorescent laser scanning confocal microscopy system (TCS SP5, Leica Microsystems). The fs laser served as the method to generate targeted damage on the plasma membrane of individual cells. The confocal microscope provided *in situ* time-lapse live imaging of the post-photoporation cellular responses, as well as the 3D visualization of the plasma membrane to be targeted for fs laser photoporation.

The fs laser (repetition rate: 80 MHz) was able to generate 100 fs laser pulses in 800 nm with an average power range of 40–120 mW. The power of the fs laser used in this study was uniformly set as 55 mW through initial calibration before each experiment. The pulsed laser beam was directed into the confocal microscope light path and tightly focused to a femtolitre focal volume at the basal plasma membrane by a $\times 63$ water immersion objective with high numerical aperture (N.A.) of 1.2. With this femtosecond laser set-up, a single site-specific perforation could be generated on the plasma membrane. Argon laser at 488 nm and He–Ne laser at 633 nm were both applied in the experiment to excite the fluorescent imaging markers of the cells. Transmitted light was detected to provide a reference bright field image.

Cell Preparation

Cell Culture and Preparation in the Normal Condition

One of the typical load-bearing cell models, the C2C12 mouse myoblast cell line was used in this study. C2C12 myoblasts (CRL-1772, ATCC Organization) were seeded in a 35 mm confocal dish (SPL Lifesciences Inc.) at a density of 50,000 cells per dish. Dulbecco's modified Eagle medium (DMEM, gibco®, Life Technologies Inc.) supplemented with 10% Fetal Bovine Serum (FBS, gibco®, Life Technologies Inc.) and 1% Penicillin streptomycin (Pen Strep, gibco®, Life Technologies Inc.) was applied as the culture medium. After cell seeding, the sample dish was placed in an incubator at 37 °C temperature with 5% carbon dioxide for 48 h to foster cell attachment and proliferation. C2C12 myoblasts could differentiate into myotubes with membrane syncytia after reaching confluence within the dish, which would make it difficult to identify the cell boundary for the purpose of this experiment. Therefore the seeding density and culture duration of the myoblasts were specially chosen to maintain the cells in the solitary form to facilitate the quantification of the morphological characteristics. The cells were then stained with calcein AM (excitation/emission maxima: 488/536 nm, Molecular Probes®, Life Technologies Inc.) for 10 min at a concentration of 1 μg/ml for signaling cell viability. After that, the medium was removed and the cells were washed 3 times using PBS. The cells were then stained with a plasma membrane dye (excitation/emission maxima: 650/680 nm, Molecular Probes®, Life Technologies Inc.) at a concentration of 5 μg/ml and incubated for another 10 min. After incubation, the medium was removed and the cells were washed 3 times. Fresh culture medium was then added into the sample dish. The cells sample was ready for laser photoporation.

H_2O_2 Treatment

Hydrogen peroxide (H_2O_2, Unichem Inc.) was employed as an extrinsic oxidant in the experiment to impose oxidative stress on the myoblasts. H_2O_2 was

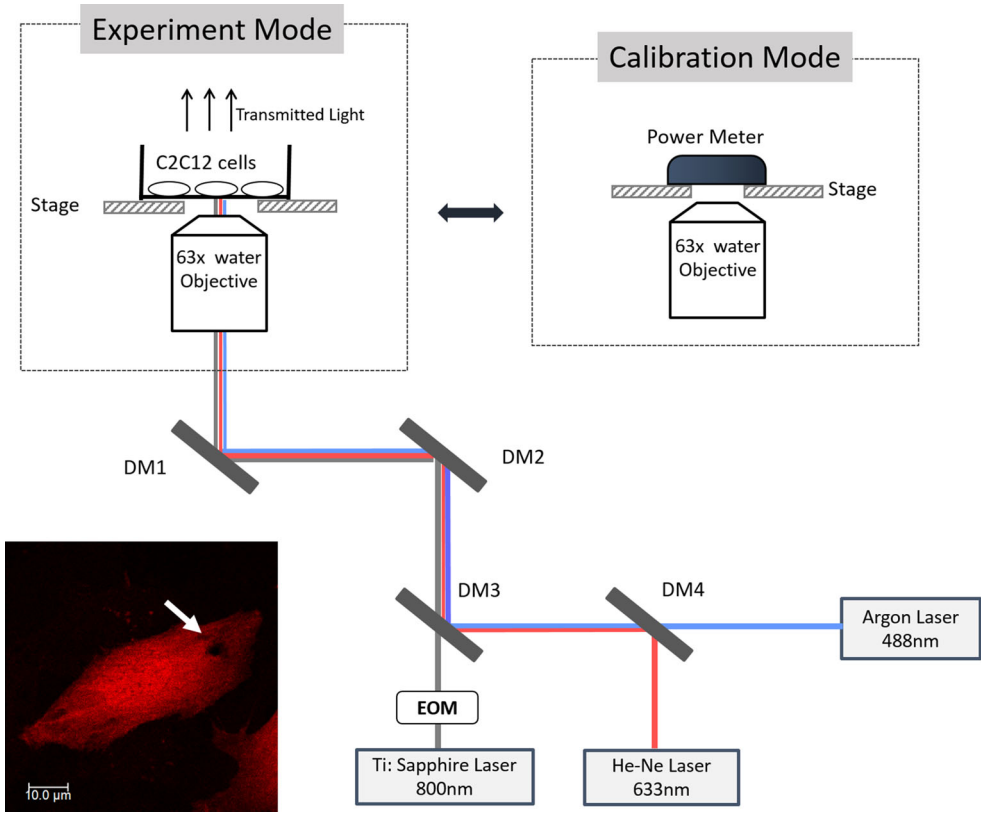

FIGURE 1. The schematic of the experimental platform. In the laser calibration mode, a power meter was placed on the stage to measure the fs laser power. During the experiment, C2C12 sample dish was placed on the stage. DM denotes dichroic mirror; EOM denotes Electro-Optic Modulator. One photoporated cell sample is shown at the bottom left corner. The fs laser induced pore is highlighted by white arrows. The criteria for the site of laser irradiation included: (a) on the basal plasma membrane; (b) generally along the long axis of the cell; (c) preferentially on the side with a larger membrane area; and (d) roughly at the midpoint between the cell boundary and the nucleus envelope.

applied to the cells at either 2 or 0.5 mM, corresponding to an earlier study of the evolution of biophysical damage on the myoblast plasma membrane.[21] Chronic exposure to H_2O_2 at the two concentrations could induce significant difference in DNA fragmentations associated with different apoptotic cell death.[22] Acute exposure at such concentrations could also cause significant alteration of the biomechanical properties of the cells.[23] Exposure durations of 1 and 24 h were selected to study the chronic and acute effects of the imposed oxidative stress. In this study, we investigated 3 oxidative conditions—0.5 mM H_2O_2 for 1 h, 0.5 mM H_2O_2 for 24 h and 2 mM H_2O_2 for 1 h. The 2 mM H_2O_2 for 24 h was not pursued because myoblasts could not survive well in such a strong and chronic oxidative environment according to a previous cell viability test.[24] For the acute H_2O_2 treatment groups (0.5 mM/1 h, 2 mM/1 h), the C2C12 cells were first seeded in a confocal dish and incubated for about 46 h. The culture medium was then replaced by the oxidative treatment medium. Afterwards, the cells were put back into the incubator for 1 h. After that, the cells were rinsed with PBS for 3 times. The H_2O_2 treated cells subsequently went through the same staining steps as the normal cells described above. For the chronic H_2O_2 treatment group (0.5 mM/24 h), the cell culture medium was replaced by the oxidative medium after 24 h incubation of the freshly seeded cells. The oxidative treatment lasted for another 24 h, all in a 37 °C and 5% carbon dioxide environment. The other experimental steps were similar to those of the acute H_2O_2 treatment group.

Fs Laser Photoporation and Imaging Protocol

Power Measurement and Calibration

A slide power meter (Thorlabs co ltd.) was employed to measure the average power irradiated on the sample. As shown in Fig. 1, the power meter was placed at the same position as the cells sample. The MaiTai HP fs laser control system was integrated with the confocal microscopic control software (Leica LCS AF). The power of the fs laser was tuned using the

LCS software system. A 10-second fs laser irradiation was executed for testing. The average irradiation power was measured by the power meter. The testing and tuning procedures were repeated several times until the specific average power (55 mW) was attained. Then the laser power was fixed in the control software and testing was conducted for another 3 times to assure the average power was stable. Once the laser power was assured stable at the target power, the fs laser was ready for the plasma membrane photoporation experiment. The laser average power was calibrated once every 2 h during the experiment, just in case that the fs laser power might be drifting during the experimental period.

Fs Laser Irradiation Protocol

After the fs laser was calibrated at the target power, the power meter was removed and the cells sample was placed on the stage. A living myoblast with calcein staining was identified under the confocal microscope. The fs laser was then targeted at a specific site on the basal plasma membrane of the myoblast for laser irradiation. A typical fs laser-induced pore on the myoblast plasma membrane was shown in Fig. 1, along with the guideline for selecting the photoporation site. The fs laser irradiation site was roughly a round spot (aspect ratio 0.9–1.1). The diameter of the fs light spot could be estimated by Rayleigh's Criterion:

$$d = \frac{0.61\lambda}{\text{N.A.}} \tag{1}$$

where λ is the wavelength of the fs laser light, N.A. is the numerical aperture of the objective. In this study, the diameter of the light spot was ~407 nm. The depth of the fs laser insult was ~369 nm. The laser irradiation time was 2 ms for all the experiments reported in this study.

Imaging Protocol

Before the fs laser irradiation, 3D volume fluorescent scanning of the cell was conducted (0.5 μm per layer) at 1.3 s/f (second per frame) to record the pre-photoporation morphology of the myoblast. The image size of each layer is 512 × 512 in pixel. Following the 2 ms fs laser irradiation, a sequence of 2D time-lapse images with a time interval of 5.2 s were acquired immediately. This real-time post-photoporation observation lasted for 5–7 min (up to the wound closure time). The 2D image size was 512 × 512 in pixel. After that, another 3D volume scanning of the cell was conducted similar to the pre-photoporation one to assess the change in the 3D morphology of the cell after photoporation damage.

Image Analysis

ImageJ software was used to quantify the cell cross-sectional images and to construct the 3D images of the cells. The 3D morphology of the investigated cells and their orthogonal sectional images (x–y cross-section, x–z cross-section, y–z cross-section) were obtained (Fig. S1).

The volume of a cell was estimated using the approximation:

$$V = \sum Ai \cdot \Delta d \tag{2}$$

where V is the cell volume, Ai is the x–y projection area of the ith scan layer, and Δd is the thickness of each scan layer (~0.5 μm).

Cell thickness was estimated by:

$$T = n \times \Delta d \tag{3}$$

where T is the cell thickness, n is the number of the x–y cross-sectional layers from the bottom to the top of a cell in the 3D volume scanning.

The 2D projected area of the nucleus (x–y section) was measured in the LAS AF Lite software (Leica). The nucleus was first fitted with an ellipse and the elliptical area was calculated. The procedure was repeated 3 times by one observer to obtain an average estimation.

Statistics

The results shown are averages of each experiment ± standard error of the mean (SEM). The significance of trends was confirmed by analysis of variance (ANOVA) and post hoc Student's t test using the GraphPad software (version 5.00). For the comparison between different treatment groups, unpaired t test was applied. For the comparison between pre- and post- photoporation characteristics of the same cells, paired t-test was applied. Correlation of two variables was evaluated using the Pearson product moment correlation coefficient (Pearson's r).

RESULTS

Cell Volume After Fs Laser Photoporation: Decreased in the Normal Cells and Increased in the H_2O_2 Treated Cells

Figure 2a shows the change percentage of the cell volumes in all the four groups. For the normal cell samples, post-photoporation cell volumes decreased by 11.4 ± 2.30%, when compared to their respective pre-photoporation volumes. Considering the relatively big variation in the initial cell volume, we reported the change percentage here. The results showed that nor-

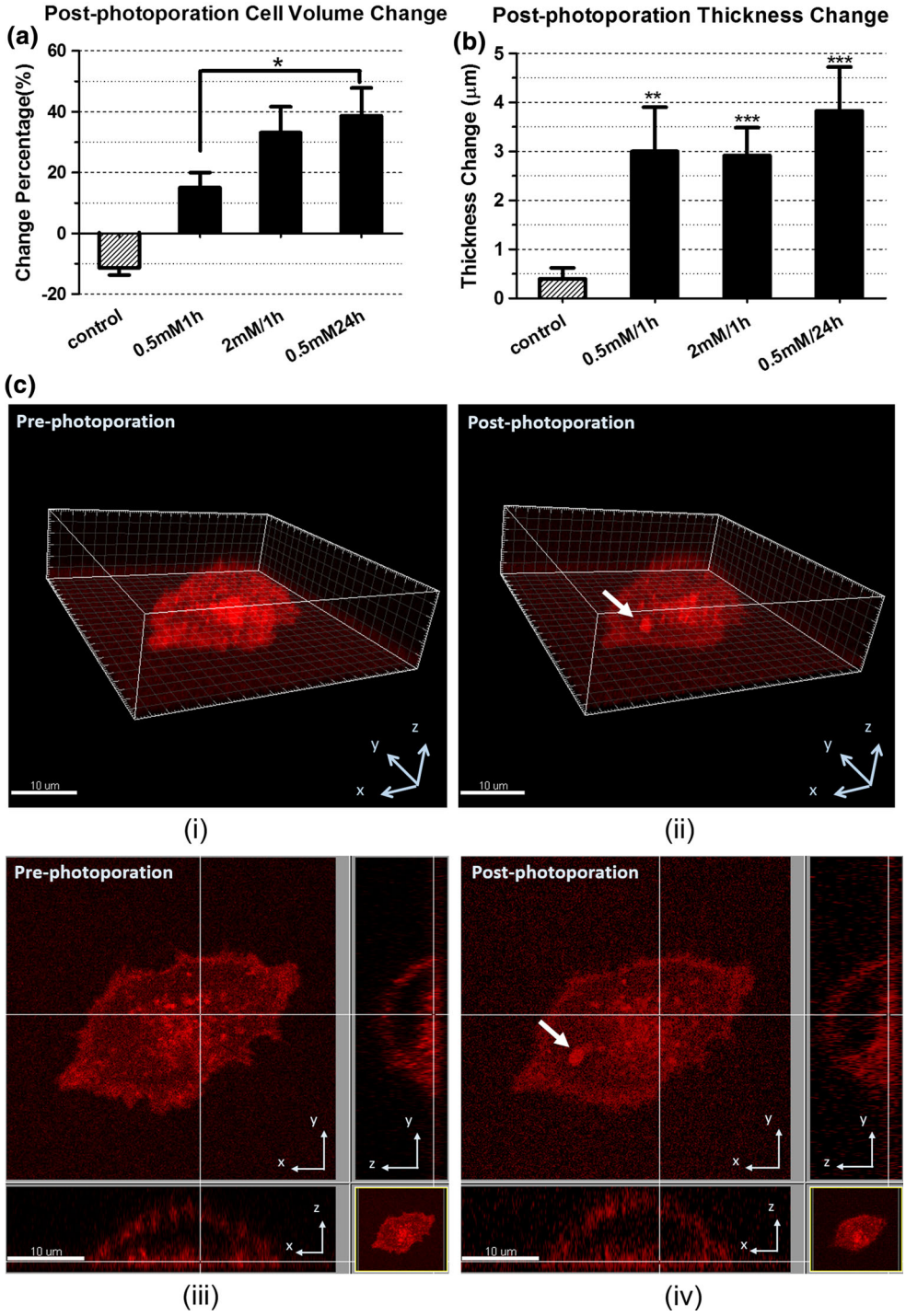

FIGURE 2. The post-photoporation morphological changes of the cells in the four groups. (a) change of cell volume; (b) change of cell thickness; (c) 3D image reconstruction of a myoblast pre-treated by 0.5 mM H_2O_2 for 1 h. (i) before photoporation and (ii) ~5 min after photoporation. (iii) and (iv) are the bottom cross-section of (i) and (ii) respectively. Bar = 10 μm. The arrows denotes the photoporation site. Quantification was based on 6 to 10 myoblasts from 3 to 4 independent experiments. (*:$p < 0.05$; **:$p < 0.01$; ***:$p < 0.001$)

mal cells shrank in response to the fs laser photoporation and the shrinkage was statistically significant (paired t test: **$p < 0.01$).

For the three oxidative groups, cell volumes increased significantly after photoporation (paired t test: *$p < 0.05$ for the 0.5 mM/1 h H_2O_2 group,

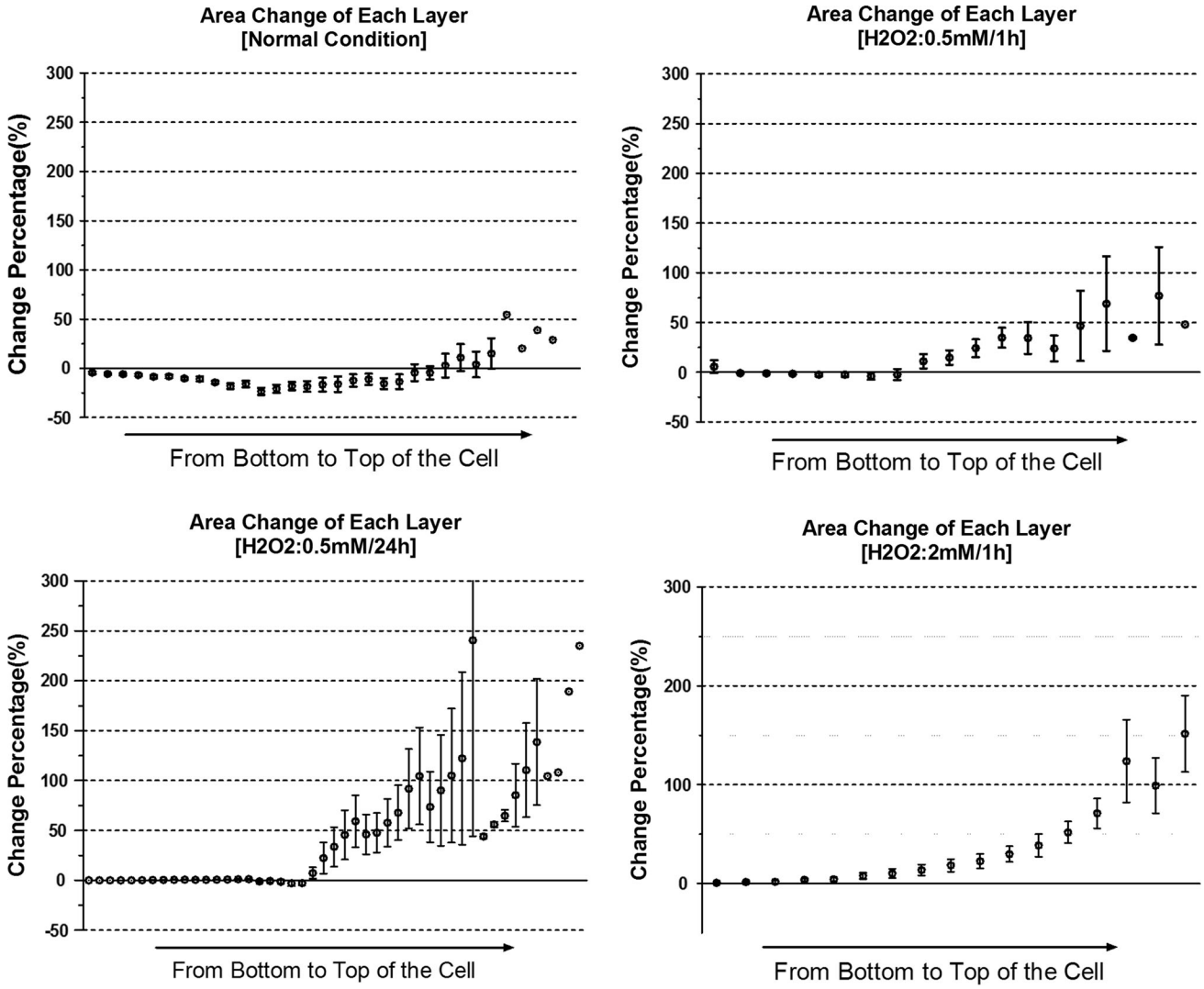

FIGURE 3. Comparison of the post-photoporation area change in each cross-sectional layer of single myoblasts in different groups. The error bar represents the SEM of the percentage changes at the same height of different cells, i.e. the same distance between the layer and the cell bottom. The isolated data points without error bar present the data of the higher layers belonging to the thickest cell. Quantification was based on the same myoblast samples in Fig. 2.

$^{**}p < 0.01$ for the 0.5 mM/24 h H_2O_2 group, $^{**}p < 0.01$ for the 2 mM/1 h H_2O_2 group). Figure 2a indicates there were critical differences between the oxidative groups and the control group. In the control group (normal condition), cells volumes went down after photoporation; while in the oxidative groups, the post-photoporation cell volumes went up. Among the three oxidative groups, the degrees of the cell volume increases differed. The increase of cell volume in the 0.5 mM/24 h H_2O_2 group was significantly higher than that in the 0.5 mM/1 h H_2O_2 group.

Cell Thickness After Fs Laser Photoporation: Remained the Same in the Normal Cells, but Became Thicker in the H_2O_2 Treated Cells

Figure 2b presents the thickness change of the four groups after photoporation. For the cells in the normal condition, there was no significant difference in the cell thickness before and after laser photoporation (paired t test: $p > 0.05$).

In the oxidative groups, all the cells became significantly thicker after fs laser photoporation (paired t test: $^{*}p < 0.05$ for the 0.5 mM/1 h H_2O_2 group, $^{**}p < 0.01$ for the 0.5 mM/24 h H_2O_2 group,

$^{**}p < 0.01$ for the 2 mM/1 h H_2O_2 group). There were no significant differences among the three oxidative groups, though the 0.5 mM/24 h H_2O_2 group apparently showed a bigger change in thickness.

Cross-Sectional Areas After Fs Laser Photoporation: Mostly Decreased in the Normal Cells, and Increased in Some Cross-Sectional Layers of the H_2O_2 Treated Cells

By comparing the pre- and post-photoporation areas of each x–y cross-sectional layer of the cells in the normal condition, most of the cross-sectional layers shrank after fs laser photoporation (Fig. 3). From the average of the change percentages of all the layers, one can see the layers closest to the bottom shrank only slightly. The shrinkage of the cross-sectional layers increased with the vertical distance from the bottom, and then decreased with this distance for layers above the mid-plane. For the layers close to the top of the cell, the sectional areas even expanded apparently relative to its pre-photoporation area. Generally, most cross-sectional areas decreased from the bottom to the top layers of the cell, except for the very few layers near the top.

On the contrary, the results of the oxidative groups showed that the areas of many cross-sectional layers of the cells increased after photoporation, except the basal layer, which showed very little change. As reflected in Fig. 3, layer areas gradually increased from the bottom to the top. Layers in the 0.5 mM/1 h group showed smaller changes, while those in the 0.5 mM/24 h group changed more distinctly.

A common phenomena in both the control and the oxidative groups was that the layers away from the bottom tended to experience bigger changes in area after fs laser damage.

Nucleus Transformation After Fs Laser Photoporation: The 2D Projected Area of the Nucleus Shrank in Both the Normal and the H_2O_2 Treated Cells

In the normal condition, the post-photoporation images of the 2D projected area of the nucleus (x–y section) shrank by 17.7 ± 3.03% comparing with the pre-photoporation images (Fig. 4b). This significant difference ($^{***}p < 0.001$) suggests the cell nucleus experienced a remarkable transformation after fs laser photoporation of the cell.

The remarkable decrease of the 2D projected area of the nucleus was also observed in the three oxidative groups subsequent to fs laser irradiation as indicated in Fig. 4b (paired t-test $^{*}p < 0.05$ for all the three groups). Concerning the post-photoporation change percentage of the x–y projected area of the nuclei, a significant difference was found between the control group and the 0.5 mM/24 h H_2O_2 group. Both the acute oxidative groups (H_2O_2 0.5 and 2 mM/1 h groups) showed no significant difference compared to the control.

Nucleus Translocation After Fs Laser Photoporation: Nucleus Moved Away from the Wound Site

Nuclei tended to move away from the damage site in the post-photoporation images, as reflected in Fig. 4a by the shift of the nucleus center and of its proximal boundary relative to the wound site. The nucleus center was defined as the geometric center of the nucleus-fitted ellipse. The distance between the nucleus center and the laser damage site (NCD) was measured to evaluate the nucleus center translocation after fs laser photoporation.

In the normal condition, the proximal boundary vertices of the nuclei apparently retreated in all the 10 cells (3.1 ± 0.31 μm). Eight out of the 10 cell samples showed NCD increase (2.2 ± 0.40 μm) after fs photoporation. In one of the exceptional cells, nucleus did not show a measurable translocation, whereas in another exceptional cell, the nucleus moved slightly towards the damage site by 0.6 μm.

For the 0.5 mM/1 h H_2O_2 group, after fs laser photoporation, the proximal boundary of the 7 sample nuclei retreated by 3.7 ± 0.97 μm. Meanwhile NCD increased by 1.7 ± 0.46 μm (Fig. 4c). The two parameters were positively correlated ($r = 0.73$).

For the 0.5 mM/24 h H_2O_2 group, the proximal boundary of the nuclei retreated by 4.9 ± 0.81 μm, while the NCD increased by 2.3 ± 0.71 μm. In one single exceptional case, the nucleus center apparently move slightly towards the damage site by 0.3 μm. On the other hand, the post-photoporation proximal boundary of this nucleus still retracted markedly from the damage site by 2.0 μm mainly. This could be due to the dramatic shrinkage of the 2D projection of the nucleus (projected area decreased by 73.3%) after laser photoporation. Despite this, the NCD change and the shift of the proximal boundary were positively correlated ($r = 0.62$).

For the 2 mM/1 h H_2O_2 group, proximal boundaries of the 6 sample nuclei retracted by 2.1 ± 0.4 μm. The post-photoporation NCD showed no significant increase. In one of the exceptional case, NCD decreased 0.8 μm. Similar to the exceptional case in the 0.5 mM/24 h group, dispite the negative NCD, the post-photoporation proximal boundary of this nucleus still retracted by 1.0 μm. The NCD change and the movement of the proximal boundary showed a moderately positive correlation ($r = 0.59$).

In both the control and the oxidative groups, the nuclei apparently moved away from the damage site, as evidenced either in term of the retraction of the proximal

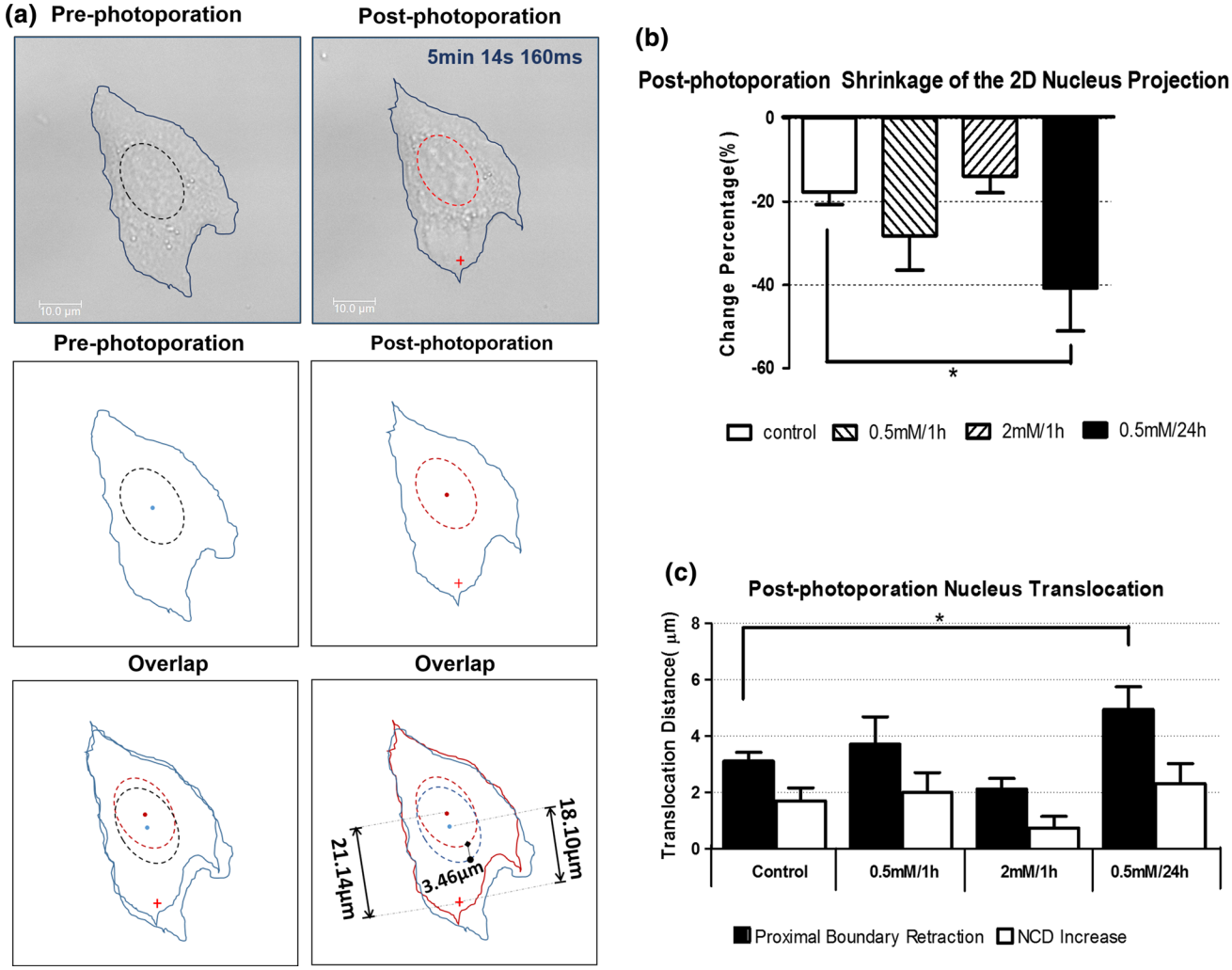

FIGURE 4. Nucleus transformation and translocation after laser photoporation. (a) The shift of the proximal boundary and NCD. The first row showed the comparison of pre-photoporation and post-photoporation bright field images. The blue lines portray the cell boundary. The dashed lines represent the nucleus-fitted ellipses. The redcross denotes the fs laser damage site. The second row delineated the sketches of the boundary of the nucleus and cell shape extracted from the bright field image. The third row was the overlay of the pre-photoporation and post-photoporation sketches. In the right sketch, the blue line portrays the pre-photoporation profile and the red line portrays the post-photoporation profile. The pre-photoporation NCD was 18.1 μm and the post-photoporation NCD was 21.1 μm. The proximal boundary translocation was 3.5 μm. (b) post-photoporation change in the 2D projected area of the nuclei in the four groups — only the 0.5 mM/24 h group showed a significant difference with the control group (*$p < 0.05$). (c) Retraction of the 2D proximal boundary of the nuclei and the NCD increase after photoporation. Control group: $n = 10$; 0.5 mM/1 h group: $n = 7$; 2 mM/1 h group: $n = 6$; 0.5 mM/24 h group: $n = 6$. Data were collected from 3 to 4 independent experiments.

boundary of the nucleus or the increase of NCD. Among the four groups, only the chronic oxidative group showed a significantly higher proximal boundary retraction than the control group. No other significant difference was found in the proximal boundary retraction nor in the NCD increase. Typically, the proximal boundary of the nucleus retracted by a larger amount than the NCD increase. In the very few cases where NCD shortened slightly, the proximal boundary still retracted after fs laser damage. This discrepancy might be either due to the dramatic cell shrinkage or owing to the challenge in defining the cell nucleus by elliptical fitting. Note that both the decrease of 2D projected area of the nuclei and the NCD increase contributed to the apparent retraction of the proximal boundary. Overall, one may say that the nucleus moved away from the laser damage site simply from the significant retraction of the proximal boundary.

DISCUSSIONS

In this study, we investigated the multiple biophysical changes of single cells after fs laser photoporation. Figure 5 schematically delineates the differences in

post-photoporation cell transformation between the cells in normal condition and those in oxidative conditions. Under normal condition, a significant decrease of cell volume was found after fs laser photoporation. This indicated that normally myoblasts underwent a cell shrinkage after membrane photoporation as indicated by the cell volume. It has been known that plasma membrane disruption is immediately followed by the transient efflux of cytoplasm and the influx of extracellular milieu.[3,9] It is highly possible that an excessive amount of the cytoplasm efflux could be one of the causes of the cell volume decrease after membrane photoporation. Also following a membrane disruption, the normal cellular responses at the wound site include the assembly and contraction of the actomyosin ring,[5,25,26] which is mainly composed of F-actin and myosin II. During the wound closure, the actomyosin contraction could reportedly drive a reorganization of the cytoskeleton and cell adhesion, which could modify cell shape during the wound healing process.[27] This could be another machinery for the cell shrinkage after photoporation, besides the excessive cytoplasm efflux. More follow-up investigations are needed to figure out which of the above two mechanisms was the major factor of the post-photoporation cell shrinkage. Meanwhile, another noticeable finding associated with the post-photoporation cell shrinkage was that such cell shrinkage seemingly came mainly from the x–y dimentional decrease. As shown in Fig. 3, the areas of most x–y cross-sectional layers decreased, while the cell thickness didn't show significant decrease after photoporation (Fig. 5a). Note that the cross-sectional layers away from the basal membrane underwent more distinct shrinkage after photoporaion. A possible explanation might be that the adhesions between the basal membrane and the culture dish effectively constrained the bottom layer for dimensional change.

The myoblasts pre-treated by the oxidative stresses showed different morphological responses after photoporation. As presented in Figs. 5b and 5d, the oxidative stresses could alter the post-photoporation morphological response from the normal shrinkage to swelling. Among the three oxidative groups, the 0.5 mM/24 h H_2O_2 group changed the most both in cell thickness and volume increase, while the 0.5 mM/1 h H_2O_2 changed the least (Figs. 2a and 2b). Our earlier study showed that the three different levels of oxidative stresses compromised the cellular resistance of myoblasts to photoporation in a similar pattern as well.[21] Together,these results indicated that chronic oxidative stress compromised the plasma membrane integrity more severely than acute oxidative stress in terms of the post-damage morphological changes. The strong acute oxidative stress compromised plasma membrane integrity greater than the mild acute oxidative stress. In general, oxidative stresses could impair the wound repair ability of the cells.

To further analyze the impact of the oxidative stresses on the myoblasts, we compared the cell morphology between the normal cells and the oxidatively treated ones before photoporation. Results showed that apart from the photoporation-induced morphological change, oxidative stresses solely may also affect cell morphology before photoporation. As shown in Fig. 5a, cell thickness was significantly lower in both two acute oxidative groups than that in the normal group. However, only the strong acute oxidative group, namely the 2 mM/1 h group showed a significantly lower cell volume. Generally, the impacts of the two acute oxidative treatments on the cells, though not to the same extent, shared a similar trend, namely cell thickness/volume decreased and the 2D projected area of the nucleus increased. Despite that cell body quantification did not reveal any significant difference between the chronic oxidative group and the control group before photoporation, it is hard to assume that the cells after the chronic oxidative stress treatment remained as functional as before the chronic oxidative treatment, judging from the cell viability after oxidative treatment[24] and the significant increase of both the cell body and thickness after photoporation (Figs. 5a and 5b). Combining the results that the maximal change percentages in cell morphology and nucleus shape were both found in this chronic oxidative group (Figs. 2a and 2b), it was likely that while maintaining a relative normal morphology after chronic oxidative treatment, the ability of these cells to maintain homeostasis after plasma membrane disruption has already been critically compromised by the oxidative stress. Indeed, comparing to the normally cultured cells in the control group, the chronic oxidative group showed the greatest disparities in both post-photoporation cell volume and thickness. Our earlier work also documented that the cells pre-treated by chronic oxidative stress held the lowest resealing ratio ($<50\%$) of fs laser induced membrane pores comparing to those treated by the acute oxidative stresses ($>90\%$).[21] Apparently, the wound responses between the chronic oxidative group and the acute oxidative groups were quite different in terms of their morphological alterations.

Our group has conducted a separate study to investigate the impacts of the oxidative stress on the cytoskeleton of C2C12 myotubes.[23,24] It was found that for the cells treated by the 0.5 mM H_2O_2/24 h chronic oxidative stress, cofilin-2, the core protein facilitating actin filament depolymerization, was up-regulated, while for the cells treated by the 2 mM H_2O_2/1 h acute oxidative stresses, cofilin-2 was down-regulated; and for the 0.5 mM H_2O_2/1 h acute oxida-

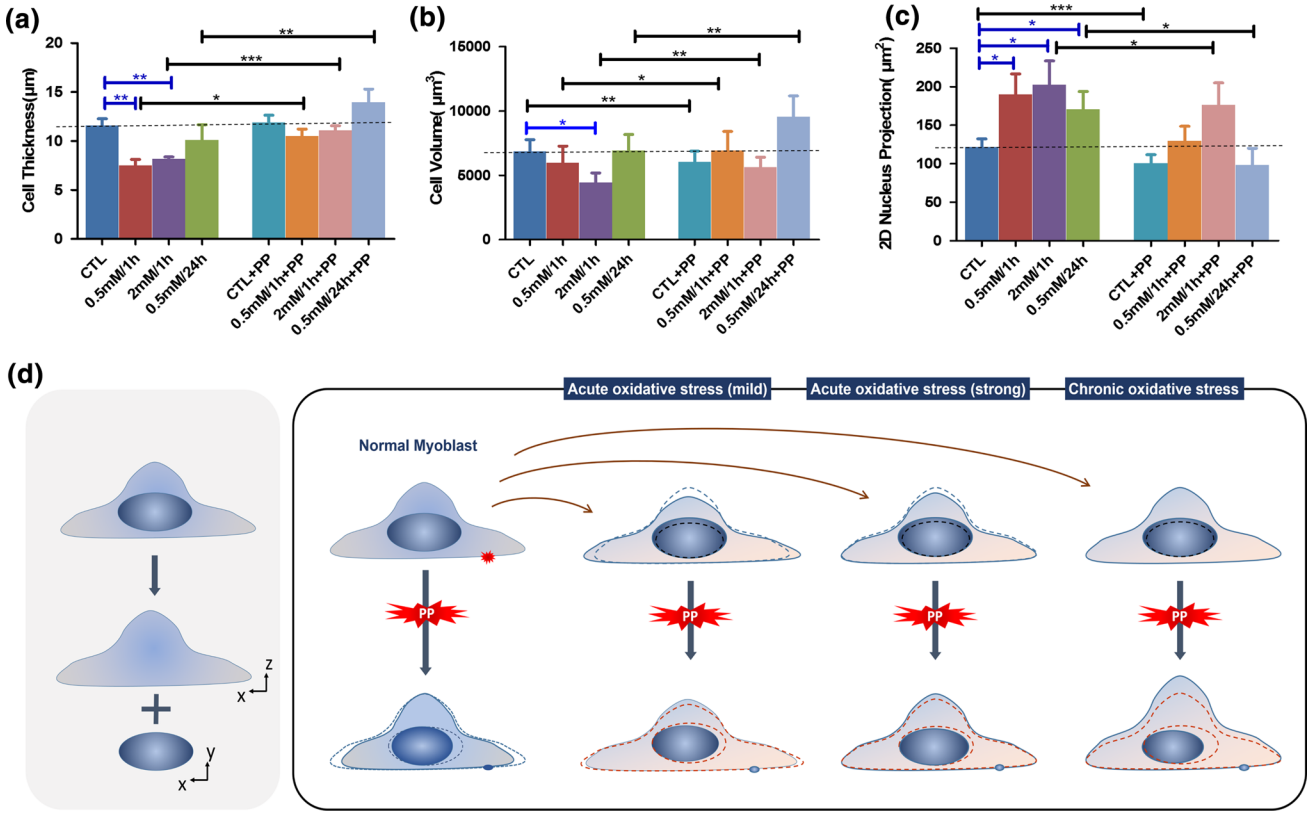

FIGURE 5. The morphology characteristics of the cells under different conditions. (a) cell thickness; (b) cell volume; (c) 2D projected area of the nucleus. CTL represents the data from the freshly cultured cell sample without prior treatment. The left four columns of each graph display the data acquired before photoporation, while the right four column are the data after photoporation. PP denotes photoporation. Quantification was based on the same myoblast samples in Fig. 4. (*:$p<0.05$; **:$p<0.01$; ***:$p<0.001$). (d) A schematic diagram of the morphological responses that illustrates how the different oxidative treatments and photoporation affected the morphology of cells and nuclei progressively. The blue lines portray the real-time morphology in each experimental step. Both the red and blue dashed lines represent the previous morphology in the last experimental step.

tive group, cells showed a small decrease in cofilin-2 but not significant. This substantiated that for the cells treated by the chronic oxidative stress, the F-actin cytoskeletal structure could be significantly compromised before photoporation in our study. This could explain why the 0.5 mM H_2O_2/24 h chronic oxidative group showed the biggest morphological alteration after photoporation. For the cells treated by 2 mM/1 h H_2O_2 and 0.5 mM/1 h, the acute oxidative stress may allow the actin cytoskeleton be maintained or even temporarily enhanced to some extent. This also conformed to the increase of the cell stiffness after such acute oxidative treatments.[24] Collectively, the previous findings of actin cytoskeleton dynamics and cell stiffness of H_2O_2 treated cells were consistent with our present findings here.

The nuclei of the myoblasts after photoporation showed multiple responses to the plasma membrane perforation, including a decrease in the x–y projected area of the nucleus and an apparent retraction away from the photoporation site. Figure 5c showed that a sole exposure to oxidative stresses might already cause considerable influences on the 2D projected area of the nucleus, as the 2D projected area of the nucleus in all the oxidative groups was significantly bigger than that in the normal group. Clearly, the nucleus morphology was sensitive to both extracellular oxidative stress and membrane perforation. Comparing the oxidative groups to the normal group, the most striking post-photoporation nucleus transformations were observed in the 0.5 mM/24 h H_2O_2 group. This may suggest a need to further study how various intracellular organelles, including the nucleus, might be affected by chronic oxidative stresses.

The direction of the nucleus transformation after photoporation was quite intriguing. The significant shrinkage of the 2D projection of the nucleus after photoporation occurred as well as the retraction of the proximal boundary away from the wound site. Furthermore, for the normal myoblasts, this 2D retraction of the nuclei also concurred with the 3D cell shrinkage. Such multiple dimensional changes coincided with the reported model that the 2D nucleus shape changes tend to mimic the changes in the whole cell morphology.[28]

In line with the model, it was demonstrated that nucleus shape changes could be induced by the transmission of stress from the moving cell boundary to the nuclear surface via the frictional interactions with the intervening cytoskeletal network.[28–30] This provides a possible explanation to our experimental observations that for the normal cells, the shrinkage of the x–y projection of the nucleus after membrane perforation was likely due to the compression by the whole cell membrane shrinkage on the x–y plane (Fig. 3) mediated by the cytoskeleton. Note that the nucleus is usually positioned roughly in the central part of a cell surrounded by the cytoskeletal networks connected via the linker of nucleoskeleton to cytoskeleton (LINC) complex. Some may speculate that cytoskeletal reorganization after membrane perforation might be the driving factor of the nuclei shape change through the LINC complex. However, there are also evidences showing that moving cell boundary was capable of driving nucleus shape change even when the cytoskeletal network and the LINC complex were disrupted.[28,29] How exactly the cytoskeletal networks and the LINC complex function to transmit forces from the transforming cell membrane to the nucleus remains an intriguing question for further study. Meanwhile, we tend to maintain the hypothesis that the post-photoporation nucleus transformation observed in the present study probably originated from the changes in the plasma membrane and was mediated by the post-photoporation cytoskeleton reorganization. For the cells pretreated with oxidative stresses, similar concordance between the whole cell deformation and the 2D nucleus shape change could be observed in the 0.5 mM/1 h H_2O_2 treatment group. However, the other two oxidative groups exhibited no clear concordance between the nucleus and the overall cell shape changes. Instead, nucleus seemingly transformed oppositely to the whole cell morphological change. As indicated in the above discussion, F-actin structure bearing the chronic oxidative stress could have been compromised. Besides that, the ERM proteins linking the cytoskeletal network to the plasma membrane structure were also down-regulated after chronic oxidative stress.[24] Lamins, one of the key proteins family in the LINC complex that helps maintain nuclear stability and modulate nuclear dynamics[31] could also be disrupted by excessive oxidative stress.[32] This may subsequently disturb the mechanotransduction signaling between nucleus and cytoskeleton.[33,34] Evidently, the dysfunctions of the cytoskeleton, the plasma membrane linker and the nucleus linker might jointly impair the mechanotransduction chain of the cells. Consequently after chronic oxidative stress, the nucleus might fail to sense the functional stress from the cytoskeleton and lost the concordance with the plasma membrane morphology. For cells treated by 2 mM/1 h H_2O_2, as the actin filament polymerization could be promoted temporally by the down-regulation of cofilin-2, it may be reasonable to hypothesize that the cytoskeleton in that abnormal situation might allow some irregular responses causing irregular changes of the nucleus. Further studies need to be conducted to investigate the detailed mechanisms.

We have successfully built a single cell model to study the biophysical responses of single myoblasts through quantification of their 3D morphology subsequent to a precise plasma membrane damage by fs laser photoporation. To further understand the present discoveries, more follow-up studies would need to be conducted. Firstly, the mechanism of cell morphological change after photoporation needs to be worked out in details. Not until then, it is difficult to further clarify the exact mechanism how oxidative stress alters these morphological responses. More biochemical underpinnings need to be included to bridge the gap between our biophysical findings and the molecular mechanisms. Secondly, the 2D transformation of the nuclei reported here were relatively rough and could be improved by 3D reconstruction of the nuclei using appropriate fluorescent probes. It was possible that the nucleus underwent significant changes in both the horizontal and vertical directions.[28] This would further inform our understanding of how the whole 3D mechanotransduction network works for the single cells. Last but not the least, it would be very interesting to use ultrafast time-lapse confocal volumetric imaging to observe the cytoskeletal changes before and after a plasma membrane disruption. The morphological alterations of cells are closely related to the changes in cytoskeleton organization. A disruption of certain local areas in the cytoskeleton such as a single stress fiber may cause a large-scale structural rearrangement of the cytoskeleton and the cell shape.[35] Such studies would undoubtedly illuminate the mechanisms of 3D mechanotransduction in cells, as well as the hierarchical mechanobiology of biophysical damages in cells and their subsequent repairs.

ELECTRONIC SUPPLEMENTARY MATERIAL

The online version of this article (doi:10.1007/s12195-017-0488-5) contains supplementary material, which is available to authorized users.

ACKNOWLEDGMENTS

The authors thank the Hong Kong Research Grants Council for the support of this research project (CUHK 415413) through its General Research Funds.

CONFLICT OF INTERESTS

Xinxing Duan, Jennifer MF Wan and Arthur FT Mak declare that they have no conflicts of interest.

ETHICAL STANDARDS

No human studies were carried out by the authors for this article. No animal studies were carried out by the authors for this article.

REFERENCES

[1]Abreu-Blanco, M. T., J. M. Verboon, and S. M. Parkhurst. Single cell wound repair: Dealing with life's little traumas. *Bioarchitecture*. 1(3):114–121, 2011.

[2]McNeil, P. L., and S. Ito. Gastrointestinal cell plasma membrane wounding and resealing in vivo. *Gastroenterology*. 96(5 Pt 1):1238–1248, 1989.

[3]Abreu-Blanco, M. T., J. J. Watts, J. M. Verboon, and S. M. Parkhurst. Cytoskeleton responses in wound repair. *Cell. Mol. Life Sci.* 69(15):2469–2483, 2012.

[4]McNeil, P. L., S. S. Vogel, K. Miyake, and M. Terasaki. Patching plasma membrane disruptions with cytoplasmic membrane. *J. Cell Sci.* 113(11):1891–1902, 2000.

[5]Mandato, C. A., and W. M. Bement. Contraction and polymerization cooperate to assemble and close actomyosin rings around Xenopus oocyte wounds. *J. Cell Biol.* 154(4):785–798, 2001.

[6]Chen, X., J. M. Wan, and C. Alfred. Sonoporation as a cellular stress: induction of morphological repression and developmental delays. *Ultrasound Med Biol.* 39(6):1075–1086, 2013.

[7]Sonnemann, K. J., and W. M. Bement. Wound repair: toward understanding and integration of single-cell and multicellular wound responses. *Annu. Rev. Cell Dev. Biol.* 27:237, 2011.

[8]McNeil, P. L., and R. A. Steinhardt. Plasma membrane disruption: repair, prevention, adaptation. *Annu. Rev. Cell Dev. Biol.* 19(1):697–731, 2003.

[9]Bansal, D., K. Miyake, S. S. Vogel, S. Groh, C.-C. Chen, R. Williamson, *et al.* Defective membrane repair in dysferlin-deficient muscular dystrophy. *Nature.* 423(6936):168–172, 2003.

[10]Davies, K. J. Oxidative stress, antioxidant defenses, and damage removal, repair, and replacement systems. *IUBMB Life*. 50(4–5):279–289, 2000.

[11]Radak, Z., A. W. Taylor, H. Ohno, and S. Goto. Adaptation to exercise-induced oxidative stress: from muscle to brain. *Exerc. Immunol. Rev.* 7:90–107, 2001.

[12]Urso, M. L., and P. M. Clarkson. Oxidative stress, exercise, and antioxidant supplementation. *Toxicology*. 189(1):41–54, 2003.

[13]Bonnard, C., A. Durand, S. Peyrol, E. Chanseaume, M.-A. Chauvin, B. Morio, *et al.* Mitochondrial dysfunction results from oxidative stress in the skeletal muscle of diet-induced insulin-resistant mice. *J. Clin. Investig.* 118(2):789–800, 2008.

[14]Aoi, W., Y. Naito, Y. Takanami, Y. Kawai, K. Sakuma, H. Ichikawa, *et al.* Oxidative stress and delayed-onset muscle damage after exercise. *Free Radic. Biol. Med.* 37(4):480–487, 2004.

[15]Powers, S. K., A. N. Kavazis, and J. M. McClung. Oxidative stress and disuse muscle atrophy. *J. Appl. Physiol.* 102(6):2389–2397, 2007.

[16]Aihara, H., and J. I. Miyazaki. Gene transfer into muscle by electroporation in vivo. *Nat. Biotechnol.* 16(9):867–870, 1998.

[17]Van Wamel, A., K. Kooiman, M. Harteveld, M. Emmer, J. Folkert, M. Versluis, *et al.* Vibrating microbubbles poking individual cells: drug transfer into cells via sonoporation. *J. Control. Release* 112(2):149–155, 2006.

[18]Malpeli, J. G. Reversible inactivation of subcortical sites by drug injection. *J. Neurosci. Methods.* 86(2):119–128, 1999.

[19]Stevenson, D., B. Agate, X. Tsampoula, P. Fischer, C. Brown, W. Sibbett, *et al.* Femtosecond optical transfection of cells: viability and efficiency. *Opt. Express.* 14(16):7125–7133, 2006.

[20]Antkowiak, M., M. L. Torres-Mapa, D. J. Stevenson, K. Dholakia, and F. J. Gunn-Moore. Femtosecond optical transfection of individual mammalian cells. *Nat. Protoc.* 8(6):1216–1233, 2013.

[21]Duan, X., K. T. Chan, K. K. Lee, and A. F. Mak. Oxidative stress and plasma membrane repair in single myoblasts after femtosecond laser photoporation. *Ann. Biomed. Eng.* 43(11):2735–2744, 2015.

[22]Siu, P. M., Y. Wang, and S. E. Alway. Apoptotic signaling induced by H_2O_2-mediated oxidative stress in differentiated C2C12 myotubes. *Life Sci.* 84(13):468–481, 2009.

[23]Wong, S. W., S. Sun, M. Cho, K. K. Lee, and F. Arthur. H2O2 exposure affects myotube stiffness and actin filament polymerization. *Ann. Biomed. Eng.* 43(5):1178–1188, 2015.

[24]Sun, S., S. Wong, A. Mak, and M. Cho. Impact of oxidative stress on cellular biomechanics and rho signaling in C2C12 myoblasts. *J. Biomech.* 47(15):3650–3656, 2014.

[25]Bement, W. M., C. A. Mandato, and M. N. Kirsch. Wound-induced assembly and closure of an actomyosin purse string in Xenopus oocytes. *Curr. Biol.* 9(11):579–587, 1999.

[26]Russo, J. M., P. Florian, L. Shen, W. V. Graham, M. S. Tretiakova, A. H. Gitter, *et al.* Distinct temporal-spatial roles for rho kinase and myosin light chain kinase in epithelial purse-string wound closure. *Gastroenterology.* 128(4):987–1001, 2005.

[27]Tamada, M., T. D. Perez, W. J. Nelson, and M. P. Sheetz. Two distinct modes of myosin assembly and dynamics during epithelial wound closure. *J. Cell Biol.* 176(1):27–33, 2007.

[28]Li, Y., D. Lovett, Q. Zhang, S. Neelam, R. A. Kuchibhotla, R. Zhu, *et al.* Moving cell boundaries drive nuclear shaping during cell spreading. *Biophys. J.* 109(4):670–686, 2015.

[29]Alam, S. G., D. Lovett, D. I. Kim, K. J. Roux, R. B. Dickinson, and T. P. Lele. The nucleus is an intracellular propagator of tensile forces in NIH 3T3 fibroblasts. *J. Cell Sci.* 128(10):1901–1911, 2015.

[30]Neelam S, Hayes PR, Zhang Q, Dickinson RB, and Lele TP. Vertical uniformity of cells and nuclei in epithelial monolayers. Scientific Reports. 2016;6.

[31]Liu, L., Q. Luo, J. Sun, and G. Song. Nucleus and nucleus-cytoskeleton connections in 3D cell migration. *Exp. Cell Res.* 348(1):56–65, 2016.

[32]Sieprath, T., R. Darwiche, and W. H. De Vos. Lamins as mediators of oxidative stress. *Biochem. Biophys. Res. Commun.* 421(4):635–639, 2012.

[33]Davidson, P. M., and J. Lammerding. Broken nuclei–lamins, nuclear mechanics, and disease. *Trends Cell Biol.* 24(4):247–256, 2014.
[34]Schreiber, K. H., and B. K. Kennedy. When lamins go bad: nuclear structure and disease. *Cell.* 152(6):1365–1375, 2013.
[35]Kumar, S., I. Z. Maxwell, A. Heisterkamp, T. R. Polte, T. P. Lele, M. Salanga, *et al*. Viscoelastic retraction of single living stress fibers and its impact on cell shape, cytoskeletal organization, and extracellular matrix mechanics. *Biophy. J.* 90(10):3762–3773, 2006.